Title

Human CTP synthase filament structure reveals the active enzyme conformation

Journal

Nature Structural & Molecular Biology, 24(6)

ISSN

1545-9993

Authors

Lynch, Eric M

Hicks, Derrick R

Shepherd, Matthew

et al.

Publication Date

2017-06-01

DOI

10.1038/nsmb.3407

Peer reviewed

nature structural & molecular biology

Human CTP synthase filament structure reveals the active enzyme conformation

Eric M Lynch[1], Derrick R Hicks[1,2], Matthew Shepherd[3], James A Endrizzi[4], Allison Maker[1], Jesse M Hansen[1,5], Rachael M Barry[6], Zemer Gitai[6], Enoch P Baldwin[4] & Justin M Kollman[1]

The universally conserved enzyme CTP synthase (CTPS) forms filaments in bacteria and eukaryotes. In bacteria, polymerization inhibits CTPS activity and is required for nucleotide homeostasis. Here we show that for human CTPS, polymerization increases catalytic activity. The cryo-EM structures of bacterial and human CTPS filaments differ considerably in overall architecture and in the conformation of the CTPS protomer, explaining the divergent consequences of polymerization on activity. The structure of human CTPS filament, the first structure of the full-length human enzyme, reveals a novel active conformation. The filament structures elucidate allosteric mechanisms of assembly and regulation that rely on a conserved conformational equilibrium. The findings may provide a mechanism for increasing human CTPS activity in response to metabolic state and challenge the assumption that metabolic filaments are generally storage forms of inactive enzymes. Allosteric regulation of CTPS polymerization by ligands likely represents a fundamental mechanism underlying assembly of other metabolic filaments.

Many metabolic enzymes undergo dynamic rearrangement into large-scale cellular structures in response to specific metabolic cues; a subset form defined filamentous structures in cells[1–7]. While the enzymes involved are generally well characterized by extensive study of their catalytic mechanisms, monomer structures, and regulation, the filamentous forms remain largely uncharacterized. Where functional data do exist, however, it is clear that metabolic filaments are important for regulating enzyme activity and for maintaining cellular homeostasis[8–12].

Filamentous polymers of CTPS appear to be universally conserved, having been observed in bacteria, yeast, flies, and human cells[1–3,13]. CTPS is a focal point for regulation of pyrimidine levels, as it directly converts UTP to CTP. We recently showed that in bacteria the product CTP drives assembly of CTPS into a filament form with lower activity[8], consistent with the role of CTP as an allosteric inhibitor of CTPS. The polymer is sensitive to substrate–product balance and can rapidly depolymerize into active tetramers in response to changes in substrate concentration. These dynamics buffer the catalytic activity of CTPS to maintain a defined ribonucleotide balance. Importantly, disruption of bacterial CTPS polymerization significantly affects cell growth and metabolism, indicating that polymerization is essential for cellular homeostasis. However, the precise molecular mechanisms of CTP-induced polymerization and inhibition of CTPS have remained unclear. Moreover, while CTPS filaments appear to be universally conserved, it is unknown whether the molecular mechanisms and functional consequences of polymerization are the same across kingdoms.

CTPS directly catalyzes the conversion of UTP to CTP. The enzyme is a homotetramer, with each monomer composed of a glutamine amidotransferase (GAT) domain and a kinase-like ammonia-ligase (AL) domain and joined by an α-helical linker[14]. Ammonia generated in the GAT domain is transferred to the AL domain and then ligated to UTP to form CTP in an ATP-hydrolysis-dependent reaction, with the allosteric regulator GTP playing a role in coupling the reactions. The mechanism of ammonia transfer remains unclear, although a conformational change that alters the relative orientations of the two catalytic domains has been proposed to open an ammonia channel between the active sites[15]. Feedback inhibition occurs through CTP binding at a site that partially overlaps with the UTP substrate-binding site[16]. The catalytic mechanism, domain structures, and the tetrameric quaternary structure of the enzyme are broadly conserved between eukaryotes and bacteria[14,15,17,18].

Given that the overall structures, catalytic mechanisms, and cellular polymerization of CTPS are conserved from bacteria to humans, it has been widely assumed that the mechanisms and functional consequences of polymerization are conserved for CTPS across species[19]. However, very little is known about the function of CTPS polymerization in eukaryotes beyond the observation that it appears to be part of a cellular stress response and to vary with developmental stage in some organisms[4,9,10,20,21]. Moreover, recent cell biological studies of CTPS polymerization in eukaryotes came to opposite conclusions about the effects of assembly on enzyme activity[9,11].

Here, we use cryo-EM, X-ray crystallography, and kinetic assays to study the allosteric regulation of human and *Escherichia coli* CTPS

[1]Department of Biochemistry, University of Washington, Seattle, Washington, USA. [2]Graduate Program in Molecular and Cellular Biology, University of Washington, Seattle, Washington, USA. [3]Department of Biology, McGill University, Montreal, Quebec, Canada. [4]Department of Molecular and Cellular Biology, University of California, Davis, Davis, California, USA. [5]Graduate Program in Biological Physics, Structure, and Design, University of Washington, Seattle, Washington, USA. [6]Department of Molecular Biology, Princeton University, Princeton, New Jersey, USA. Correspondence should be addressed to J.M.K. (jkoll@uw.edu).

Received 18 January; accepted 6 April; published online 1 May 2017; doi:10.1038/nsmb.3407

filaments. We demonstrate that human CTPS filaments assemble in the presence of substrates, have increased catalytic activity, and reveal a novel active conformation of CTPS. Further, we show that both human and *E. coli* CTPS undergo a conserved conformational cycle controlled by substrate and product binding but have opposite determinants for filament assembly. Given the importance of human CTPS as a target for cancer and immunosuppressive drugs and of bacterial CTPS as a target for antiparasitic treatments, these molecular insights into CTPS structure and allostery may provide novel opportunities to disrupt its function and regulation[22–26].

RESULTS

Structure of the ecCTPS filament

To elucidate the mechanism of CTP-induced filament assembly in *E. coli* CTPS (ecCTPS), we determined the structure of CTP- and ADP-bound ecCTPS filaments at 4.6-Å resolution by cryo-EM (**Fig. 1**, **Table 1** and **Supplementary Fig. 1**). The ecCTPS filament consists of stacked tetramers that interact through their GAT and linker domains. The tetramer interface is reorganized relative to previous ecCTPS tetramer crystal structures in the apo conformation[14,16], bringing the CTPS subunits into closer contact around the bound CTP (**Fig. 1c**,**d**). It was unclear, however, whether this novel ecCTPS conformation was a cause or consequence of filament assembly.

To distinguish between these possibilities, we solved a new ecCTPS–CTP co-crystal structure (**Table 2**) that reveals a tetramer with quaternary packing nearly identical to that which we observe in the filament (**Fig. 1e**). The fact that we observe the same tetramer conformation in the filament and in a crystal without filament-assembly contacts supports the notion that CTP binding allosterically controls ecCTPS assembly by directly inducing a filament-competent conformation of ecCTPS.

The conformational changes between this novel tetramer conformation and the apo state are almost entirely rigid-body motions, with the subunits in each state nearly the same (<0.5 Å C_α r.m.s. deviation) but with one exception: helix 218–228 is shifted 3.6 Å closer to the CTP bound on an adjacent monomer so that Phe227 packs against the CTP base. This shift also repositions Asn229 at the base of helix 218–228, creating a new hydrogen-bond network with Arg158 and Glu155 across the tetramer interface, likely stabilizing the filament conformation (**Supplementary Fig. 2**). We previously reported that E155K, a mutation associated with drug resistance through relief of CTPS inhibition[27], cannot assemble filaments[8]. Our new structure suggests this glutamate-to-lysine mutation interferes with the hydrogen-bond network that occurs across the tetramer interfaces in the inhibited conformation. These changes alter the relative orientations of the polymerization interfaces and position them to allow assembly only in the CTP-bound state (**Fig. 1f**,**g**, **Supplementary Videos 1** and **2**).

Allosteric inhibition of ecCTPS in the filament

We next sought to establish the mechanism of polymerization-induced inhibition of ecCTPS. We considered three possibilities: that substrates are occluded from the active site by assembly contacts, that the filament sterically blocks a conformational change necessary for ammonia transfer, and that the conformation of CTPS in the filament is allosterically inhibitory.

To test these possibilities, we first sought to decouple ecCTPS polymerization from CTP binding by engineering cysteine disulfide crosslinks at filament-assembly interfaces (ecCTPS^{CC}). Under nonreducing conditions, ecCTPS^{CC} spontaneously polymerizes without nucleotides, and its structure is identical to the wild-type structure minus

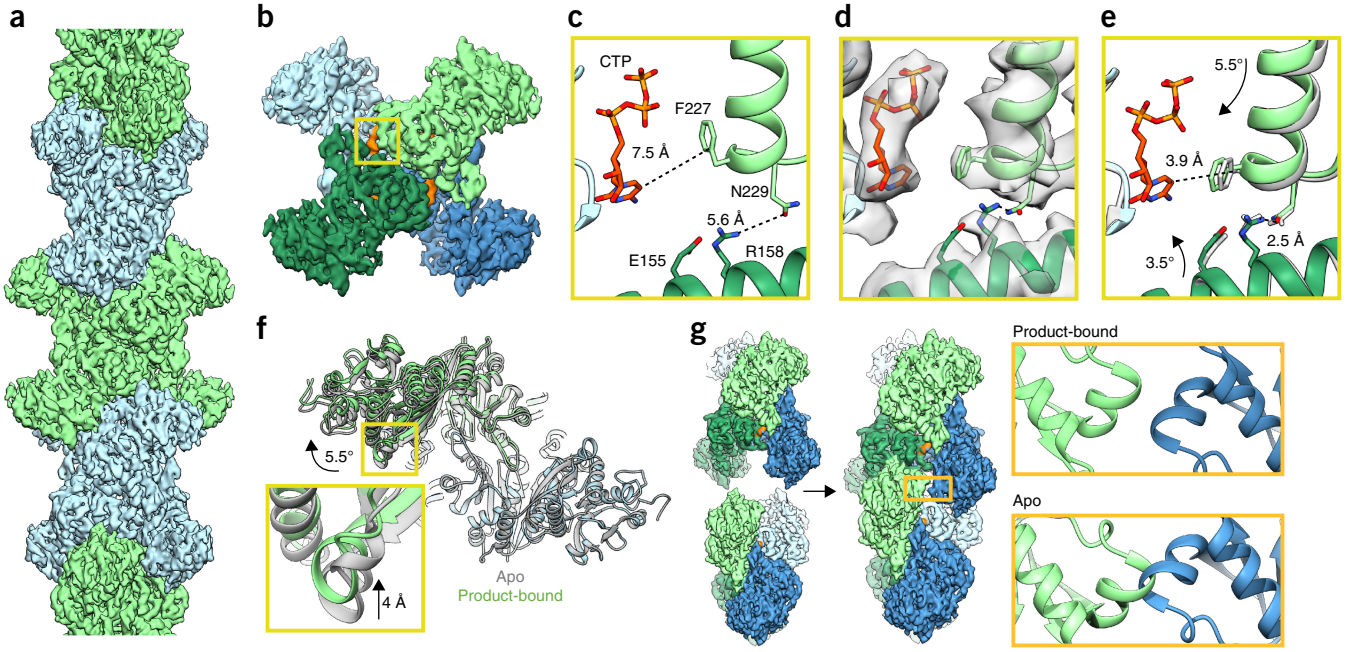

Figure 1 Mechanism of ecCTPS assembly. (**a**) Cryo-EM reconstruction of ecCTPS filament at 4.6-Å resolution. (**b**) A single ecCTPS tetramer from the filament, colored by protomer (blue and green) and nucleotide density highlighted in orange. (**c**) The inhibitory CTP binding site in apo-ecCTPS with CTP soaked into the crystals (PDB 2AD5). (**d**) The inhibitory CTP binding site in the cryo-EM structure shows compaction of the tetramer around CTP. (**e**) Overlay of the filament structure (gray) with the structure of ecCTPS co-crystallized with CTP (color). Arrows indicate the rotation of subunits relative to the apo conformation in **c**. (**f**) Overlay of the apo-ecCTPS crystal structure (gray) with the CTP-bound filament structure (color). The protomers on the lower right are superposed, revealing a rotation of 5.5° and a 4-Å translation in the positions of the protomers on the upper left. (**g**) Filament assembly contacts between ecCTPS tetramers can only be made in the novel CTP-bound conformation, as superposition of two apo tetramers would result in backbone clashing at the GAT contact site.

Table 1 EM data collection and refinement statistics

	ecCTPS filament (EMD-8504, PDB 5U3C)	hCTPS1 filament (EMD-8474, PDB 5U03)	ecCTPS tetramer (EMD-8475, PDB 5U05)	ecCTPS-CC (products) (EMD-8513, PDB 5U6R	ecCTPS-CC (substrates) (EMD-8491)	ecCTPS-CC (apo) (EMD-8490)	hCTPS1-H355A tetramer (EMD-8476)
Data collection							
Electron microscope	Polara	TF20	TF20	TF20	TF20	TF20	Spirit
Voltage (kV)	300	200	200	200	200	200	120
Electron detector	K2 summit	K2 summit	K2 summit	K2 summit	K2 summit	K2 summit	Ultrascan CCD
Electron dose (e^-/Å^2)	34	45	68	45	45	45	30
Pixel size (Å)	1.22	1.26	1.26	1.26	1.26	1.26	2.07
Reconstruction							
Point group symmetry	D2	D2	D2	D2	D2	D2	D2
Refined helical symmetry	48.5°, 81.6 Å	60.6°, 104.1 Å		48.2°, 82.1 Å	50.6°, 83.5 Å	48.2°, 82.3 Å	–
Particles	8,622	24,880	6,407	31,170	7,135	13,715	4,413
Resolution (0.143 fsc) (Å)	4.6	6.1	7.9	5.7	8.6	7.6	17
Refinement							
Initial model used	PDB 2AD5	PDB 2VO1, 2VKT	PDB 2AD5	PDB 2AD5			
Model composition							
Protein residues	534	559	534	534			
Ligands	CTP, ADP, Mg	UTP, ATP, Mg		CTP, ADP, Mg			
Validation							
Clashscore	2	4	14	2			
Poor rotamers (%)	0.1	0.2	0.1	0.1			
Ramachandran plot							
Favored (%)	94	96	94	94			
Allowed (%)	4	4	4	4			
Outliers (%)	1	1	1	1			

nucleotides (**Fig. 2a–d**). Under reducing conditions, unassembled ecCTPS^{CC} is as active as the wild-type enzyme, but apo-ecCTPS^{CC} filaments preassembled under nonreducing conditions exhibit a five-fold reduction in activity relative to free tetramers, indicating that filament assembly directly inhibits enzymatic activity (**Fig. 2e**).

When products (CTP and ADP) are soaked into preassembled ecCTPS^{CC} filaments, clear density is observed for the nucleotides in cryo-EM reconstructions, ruling out nucleotide occlusion as a mechanism of inhibition (**Fig. 2f**). To test whether filaments impair ammonia transfer between active sites, we measured the activity of ecCTPS^{CC} filaments after adding ammonia directly as a substrate. Under these conditions, ecCTPS^{CC} exhibited the same reduction in activity as the wild type, indicating that inhibition within the filament is not solely the result of an inability to couple the GAT and AL reactions. Finally, we tested whether ecCTPS^{CC} filaments could bind substrates (UTP and ATP) by soaking preassembled filaments with saturating concentrations of nucleotides. Under these conditions, no density is observed for UTP in the active site (**Fig. 2f**), suggesting reduced affinity for substrates in the filament conformation. Together, these results indicate that polymerization allosterically regulates ecCTPS activity by stabilizing an intrinsically lower-activity state upon incorporation into filaments, independent of CTP binding.

Assembly and activity of hCTPS polymer

Surprisingly, we found that purified human CTP synthase 1 (hCTPS1) polymerizes in the presence of UTP and ATP substrates but not in the presence of CTP and ADP products, exactly the opposite behavior to that observed with ecCTPS (**Fig. 3a**). hCTPS1 filaments were stable in the presence of UTP, ATP, and GTP, but they disassembled over time upon addition of glutamine, presumably as a result of accumulation of CTP product from the complete synthesis reaction (**Supplementary Fig. 3a**). Indeed, adding CTP directly to filaments assembled with substrates also resulted in disassembly, while filaments assembled with UTP, the nonhydrolyzable ATP analog AMP-PNP, and GTP were stable following glutamine addition, owing to a lack of CTP synthesis (**Supplementary Fig. 3b,c**).

Table 2 Data collection and refinement statistics

	ecCTPS CTP-bound (PDB 5TKV)
Data collection	
Space group	$P2_12_12$
Cell dimensions	
a, *b*, *c* (Å)	159.16, 110.68, 129.49
α, β, γ (°)	90.00, 90.00, 90.00
Resolution (Å)	30.0–2.70 (2.82–2.70)[a]
R_{merge}	0.092 (0.310)
$I/\sigma(I)$	11.2 (3.1)
Completeness (%)	98.3 (99.0)
Redundancy	3.4 (3.2)
Refinement	
Resolution (Å)	29.8–2.70
No. reflections	59,184/3,159
R_{work}/R_{free}	0.158/0.208
No. atoms	8,827
Protein	8,305
Ligand/ion (CTP/Mg)	158
Water	364
B factors (Å^2)	
Protein	46
Ligand/ion (CTP/Mg)	43
Water	47
R.m.s. deviations	
Bond lengths (Å)	0.0156
Bond angles (°)	1.94

[a]Single crystal. Values in parentheses are for highest-resolution shell.

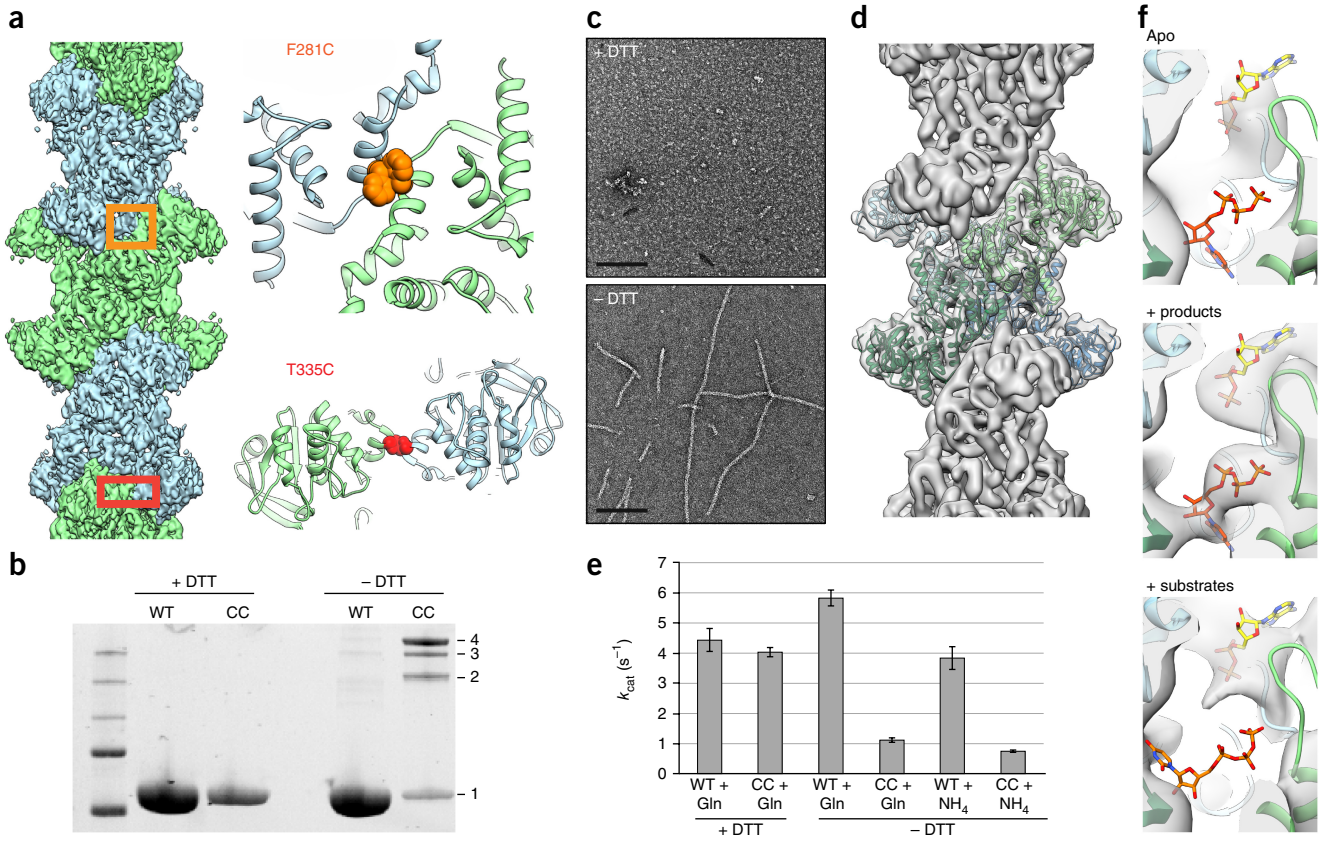

Figure 2 Engineered disulfides drive ecCTPS assembly and inhibit activity. (**a**) Design of the ecCTPS^{CC} construct, showing the locations of cysteine mutations at F281 and T335 in the linker–linker and GAT–GAT interfaces, respectively. (**b**) SDS-PAGE gel of ecCTPS wild-type (WT) and cysteine-cross-linked (CC) construct under reducing and nonreducing conditions. Under nonreducing conditions, crosslinks are introduced between protomers resulting in dimers (2), trimers (3), and tetramers (4). (**c**) Negative-stain images of apo-ecCTPS^{CC} under reducing (+ DTT) and nonreducing (– DTT) conditions. Scale bars are 200 nm. (**d**) Cryo-EM reconstruction of ecCTPS^{CC} at 5.7-Å resolution. (**e**) The activity of ecCTPS WT and CC constructs were measured under reducing (+ DTT) and nonreducing (– DTT) conditions, using either glutamine (+ Gln) or ammonium phosphate (+ NH_4) as substrates. Values are mean and s.d. from triplicate experiments. (**f**) The active site cryo-EM density from filament structures with no nucleotides present (apo), with products soaked into preformed filaments, or with substrates soaked into preformed filaments. Clear density can be seen for products, while there is no density in the overlapping CTP and UTP sites when substrates are added, suggesting the filament conformation is intrinsically inhibited.

To understand how the universally conserved CTPS enzyme could have opposite determinants for filament assembly in bacteria and humans, we solved the cryo-EM structure of hCTPS1 filaments assembled in the presence of substrates UTP and ATP and the allosteric effector GTP at 6.1-Å resolution (**Fig. 3b**,**c**, **Table 1**, **Supplementary Fig. 4**). The UTP–ATP–GTP combination was selected for structure determination as it gave the most robust polymerization of hCTPS1. Like ecCTPS, hCTPS1 is composed of stacked tetramers, but beyond this, the structures differ in their assembly contacts, tetramer interfaces, and protomer conformations. hCTPS1 filament assembly is mediated primarily by an insert in the GAT domain that appeared early in eukaryotic evolution (**Fig. 3d**, **Supplementary Fig. 5a**). This GAT–GAT assembly interaction, which is also observed in the crystal packing of existing structures of isolated hCTPS2 GAT domains (**Fig. 3e**), uses a completely different interface from filament assembly in the *E. coli* enzyme and accounts for the drastic differences in filament architecture between species. There may be additional assembly contacts between C-terminal densities that are predicted to be disordered and are poorly resolved in the cryo-EM structure (**Supplementary Fig. 4g**). Like ecCTPS, hCTPS1 assembly is allosterically controlled, but in this case, a novel substrate-bound conformation drives polymerization.

To test the biochemical consequences of polymerization, we mutated a single conserved histidine in the hCTPS1 GAT-domain helical insert (H355A). Unlike the wild-type enzyme, hCTPS1-H355A completely failed to polymerize in the presence of UTP, ATP, and GTP (**Fig. 3a**, **Supplementary Fig. 5b**). A negative-stain reconstruction of hCTPS1-H355A under these conditions confirmed that the overall tetramer structure, which is necessary for CTPS activity, was not affected by the H355A mutation (**Supplementary Fig. 5c**). However, the H355A mutation led to a six-fold reduction in hCTPS1 activity (**Fig. 3f**), indicating that hCTPS1 activity is enhanced upon subunit assembly into filaments, likely because hCTPS1 is locked in a more active conformation. This assembly of active polymers is in contrast with the suggestion from previous work, including our own description of the ecCTPS filament, that these structures generally function as inactive reservoirs of metabolic capacity[1,8,10,20]. Rather, in some instances, it seems that there may be more complex regulatory schemes in which large-scale polymerization functions to boost enzyme activity.

hCTPS filament structure

The hCTPS1 filament structure provides the first view of any CTPS in the substrate-bound active state, which differs from all existing CTPS

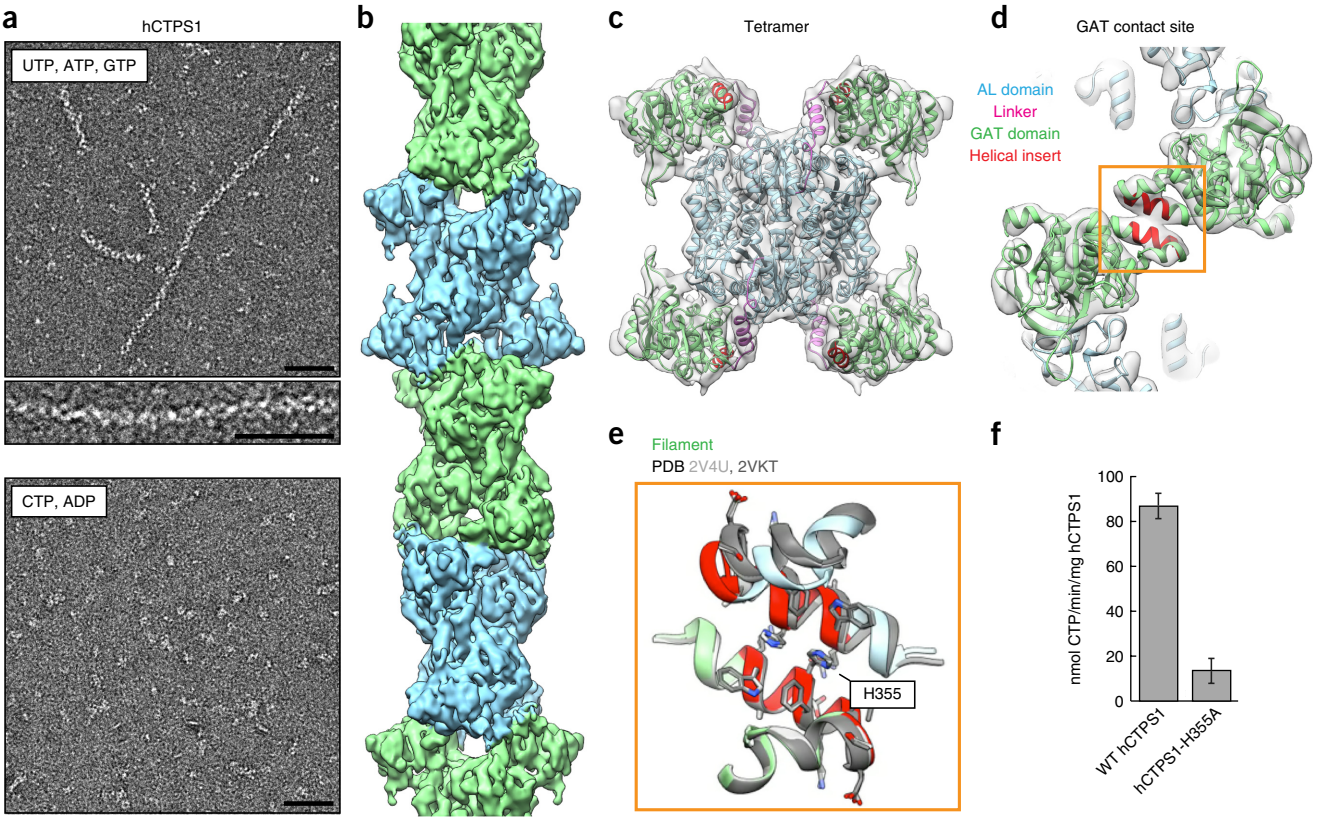

Figure 3 hCTPS1 filaments assemble with substrates and are catalytically active. (**a**) hCTPS1 polymerizes in the presence of substrates but not in the presence of products. Scale bars are 50 nm. (**b**) 6.1-Å cryo-EM map of the hCTPS1 filament, colored by tetramer subunit. (**c**) Model of the hCTPS1 tetramer fit into the cryo-EM map, colored by domain. (**d**) GAT domain contact site in the hCTPS1 filament, with the eukaryotic helical insert shown in red. (**e**) The hCTPS1 filament GAT contact site (color) is also observed in crystal structures of the hCTPS2 GAT domain (gray, PDB 2V4U and 2VKT). (**f**) WT hCTPS1 is more active than the hCTPS1-H355A nonpolymerizing mutant. Values are mean and s.d. from triplicate experiments.

structures in both the tetramerization interface and the protomer conformation (**Fig. 4**). Density for ATP and UTP substrates is clearly visible in the cryo-EM map, indicating that the hCTPS1 filaments are primed for catalysis upon addition of glutamine (**Fig. 4b**). This is consistent with the observation that metabolic filaments assemble in response to glutamine deprivation in cells[21]. Compared with CTPS structures in the inactive state, including the crystal structure of the hCTPS1 AL-domain tetramer, which exhibits analogous packing to that of helices 221–228 and 149–164 in PDB 5TKV, the active hCTPS1 tetramer is extended along the filament axis and compressed perpendicular to the filament axis by approximately 6 Å and 5 Å, respectively (**Supplementary Videos 3** and **4**), owing to rearrangements of the tetramer interface (**Fig. 4c**).

Within each hCTPS1 protomer, there is a large conformational change arising from an approximately 10° rotation between the GAT and AL domains relative to all previously reported full-length CTPS structures (**Fig. 4d**,**e**). The rotation is necessary to position the GAT domains for polymerization. In addition, the rotation appears to align two cavities within the GAT and AL domains to form a tunnel. The resolution of our cryo-EM structure is insufficient to clearly describe the nature of this tunnel, but it may function to facilitate ammonia transfer between the two active sites, similar to ammonia tunnels described in other enzymes[28] (**Fig. 4f**,**g**). This would be consistent with earlier predictions that a conformational change is required for ammonia transfer and coupling the GAT and AL reactions[14,15].

CTPS conformational states are conserved across kingdoms

We hypothesized that the conformation observed in the hCTPS1 filament is a generally conserved active conformation of the enzyme. However, as there were no previous full-length structures of hCTPS1, we could not rule out the possibility that the unique conformation was specific to the human enzyme. To determine whether ecCTPS adopts the same conformation on substrate binding, we determined the structure of the ecCTPS tetramer bound to UTP and AMP-PNP by cryo-EM at 8 Å (**Fig. 5a**,**b**, **Table 1**). The structure has the same overall conformation as the active hCTPS1 filament both at the tetramer interface (**Fig. 5c**, **Supplementary Videos 3** and **4**) and in the rotation between the AL and GAT domains (**Fig. 5d**,**e**), confirming that the conformational states of CTPS are conserved from bacteria to humans.

DISCUSSION

The structures of human and bacterial CTPS filaments suggest a model for the allosteric regulation of CTPS polymerization. The conformational equilibrium between apo, substrate-bound, and product-bound states of the CTPS tetramer is universally conserved, while evolutionary divergence at polymerization interfaces has reversed the determinants for filament assembly. The inactive product-bound conformation is stabilized in bacterial filaments, while the active substrate-bound conformation is stabilized in eukaryotic filaments (**Fig. 5f**). For both filament types, polymerization may mediate a more cooperative transition between high- and low-activity states, providing more switch-like

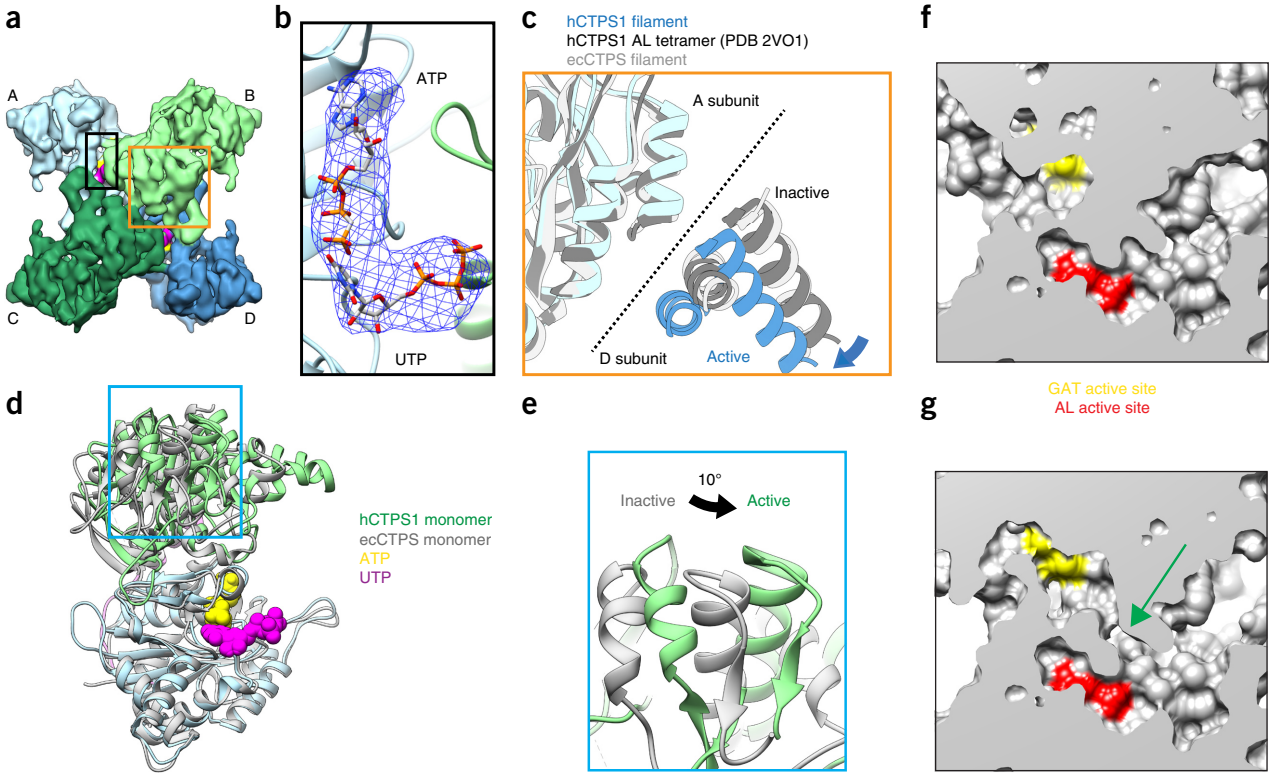

Figure 4 hCTPS1 filaments reveal the active conformation of CTP synthase. (**a**) Cryo-EM structure of the hCTPS1 tetramer in the active filament conformation. Protomers A–D are shown in different colors. (**b**) Zoomed-in view of the black box in **a**, showing the active site with atomic models fit into the cryo-EM map. A difference map (blue mesh) calculated between an apo model of the hCTPS1 filament and the hCTPS1 filament cryo-EM map reveals strong density in the active site, which was modeled to UTP and ATP. (**c**) Zoomed-in view of the orange box from **a**, showing the tetramer interface with three structures aligned on the AL domain of subunit A. The active hCTPS1 structure is extended across the tetramer interface when compared with structures of the inhibited ecCTPS filament as well as the hCTPS1 AL-domain tetramer (PDB 2VO1). (**d**) Atomic models of monomers fit to the active hCTPS1 filament (color) and the inhibited ecCTPS filament (gray), aligned on the AL domain. In the active hCTPS1 conformation, the GAT domain is rotated relative to the AL domain, bringing the two active sites closer together. (**e**) Zoomed-in view of the blue box in **d**, showing the 10° rotation of the GAT domain in the active hCTPS1 structure. (**f**,**g**) Comparison of surface representations of the atomic models of hCTPS1 in the inhibited (**f**) and active (**g**) conformations reveals an opening (green arrow) between the GAT (yellow) and AL (red) active sites.

behavior in response to small changes in substrate and product concentrations[8]. What remains unclear is the relative advantage of stabilizing hCTPS in an active conformation in the polymer. One possibility is that stabilizing the polymer under conditions of cellular stress keeps the bulk of hCTPS in a state primed for maximal activity immediately on return to normal growth conditions.

Both hCTPS and ecCTPS polymerize through association of their GAT domains. A short helical insertion at this interface both provides the primary assembly interface in hCTPS and prevents hCTPS from assembling with ecCTPS-like contacts (**Fig. 4d**,**e**, **Supplementary Fig. 4f**). The approximately ten-residue insertion appeared during early eukaryotic evolution, as only a few early-diverging single-celled lineages lack the insert. This raises the interesting question of how the two different filament forms evolved. One possibility is that CTPS of early eukaryotes formed inhibitory filaments like those of bacteria, and the appearance of the GAT insert switched the filaments to an active state. An alternative is that CTPS polymerization arose independently in bacterial and eukaryotic lineages, so that the appearance of polymerization as being a deeply conserved feature of CTPS actually reflects the independent evolution of CTPS filaments. This may be the more likely scenario, as the appearance of filamentous forms of so many different metabolic enzymes in many different lineages suggests that this is a relatively common evolutionary strategy. Investigating the role of polymerization in earlier-diverging eukaryotes, many of them human pathogens, will be necessary to clarify the evolutionary history of CTPS filaments.

For the many different metabolic enzymes that form filaments, it seems likely that in many cases, like with CTPS, binding of substrates or other ligands allosterically regulates assembly. Moreover, the ability to interconvert between dispersed and polymeric enzyme forms with different intrinsic activities may provide a general mechanism for regulating or localizing metabolic activity under complex cellular conditions. For example, CTPS activity is also regulated by phosphorylation[29–32], raising the possibility that post-translational modifications could modulate CTPS activity by influencing filament assembly, shifting the equilibrium between polymers and free tetramers to tune the total level of enzyme activity, independent of substrate and product concentrations. Similarly, binding partners may influence assembly or disassembly of CTPS filaments. This would be analogous to cytoskeletal systems like actin filaments and microtubules in which substrate binding and hydrolysis drive intrinsic polymer dynamics, but multiple factors interact to influence the timing and location of assembly. Indeed, CTPS filaments co-localize with other metabolic and signaling enzymes[4,9], suggesting that cellular factors may specifically recognize and interact with metabolic polymers.

Several cell biological studies have shown that eukaryotic CTPS filaments assemble in response to nutrient stress and at particular developmental stages[4,9–11,20,21]. Although some of these studies have

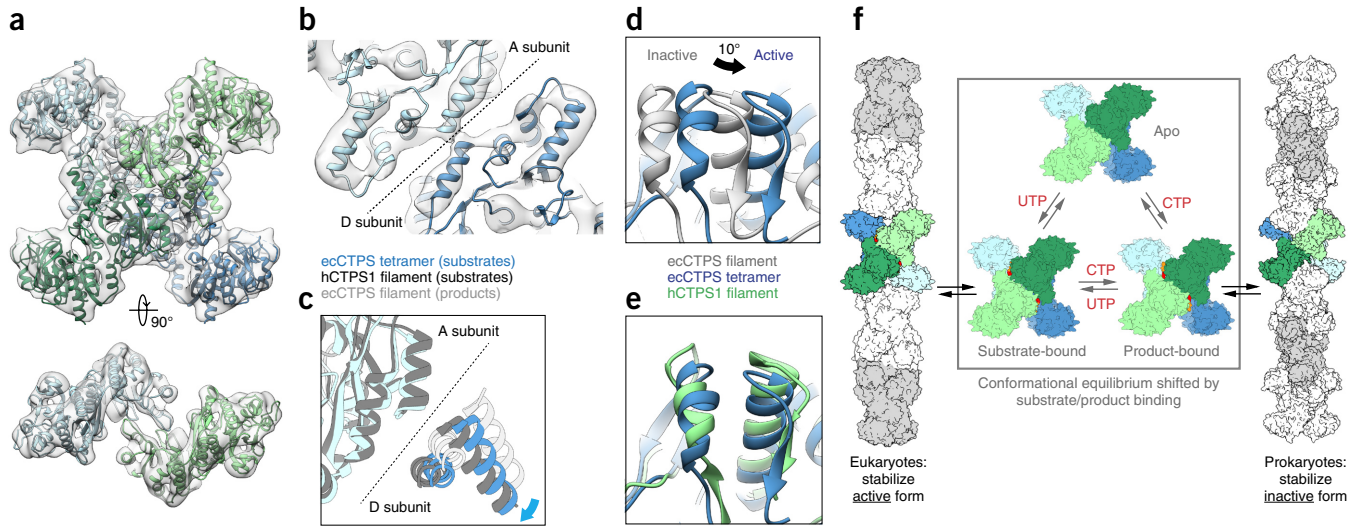

Figure 5 ecCTPS and hCTPS1 undergo a conserved conformational cycle controlled by substrate and product binding. (**a**) 8-Å cryo-EM map of substrate-bound ecCTPS (gray), fit with an atomic model (colored by protomer). (**b**) The tetramer interface in the ecCTPS cryo-EM map (gray) fit with an atomic model (color). Individual helices are clearly visible. (**c**) Comparison of the tetramer interface in the active ecCTPS tetramer conformation (blue), active hCTPS1 filament conformation (dark gray), and inactive ecCTPS filament conformation (light gray). Corresponds to the same view shown in **Figure 4c**. (**d**) 10° rotation of the ecCTPS GAT domain in the active tetramer conformation (blue) relative to the inactive filament conformation (gray). Corresponds to the same view shown in **Figure 4e**. (**e**) The same view as in **d**, comparing the active ecCTPS (blue) and hCTPS1 (green) GAT-domain rotations. (**f**) Model for the allosteric regulation of CTPS filament assembly. ecCTPS and hCTPS1 undergo a conserved conformation cycle but have opposite determinants for filament assembly.

suggested that eukaryotic CTPS filaments may be composed of catalytically inactive dimers[11,20], our work here demonstrates that isolated hCTPS filaments are polymers of active substrate-bound tetramers. Consistent with our results, CTPS in *Drosophila* germ cells forms filaments at developmental stages with a high demand for CTP, and a constitutively active mutant of hCTPS forms filaments under conditions where the wild-type protein is diffuse throughout the cytoplasm[9]. Experiments in human cells have also shown that metabolic filaments assemble in response to glutamine deprivation and disassemble upon glutamine addition[21], an effect which we observe here with purified hCTPS1.

Phosphorylation at various sites is known to modulate eukaryotic CTPS activity, leading to changes in cellular concentrations of CTP and phospholipids[29,31,32]. Multiple phosphorylation sites are located in the C-terminal tail of hCTPS1 (ref. 30), which may form assembly contacts in the hCTPS1 filament. It will therefore be interesting to investigate whether phosphorylation has a direct effect on hCTPS1 polymerization, and how enzyme regulation by polymerization is integrated into other regulatory pathways. The CTPS filament structures presented here will provide a mechanistic basis for future investigations of the cellular consequences of polymerization.

METHODS

Methods, including statements of data availability and any associated accession codes and references, are available in the online version of the paper.

ACKNOWLEDGMENTS

The authors are grateful to G. Carman (Rutgers University) for the hCTPS1-expressing *S. cerevisiae* strain. This work was supported by the US National Institutes of Health (R01 GM118396 to J.M.K.) and the Human Frontier Science Program (RGY0076/2013 to Z.G. and J.M.K.). Use of the Stanford Synchrotron Radiation Lightsource, SLAC National Accelerator Laboratory, is supported by the US Department of Energy, Office of Science, Office of Basic Energy Sciences, under Contract No. DE-AC02-76SF00515. The SSRL Structural Molecular Biology Program is supported by the DOE Office of Biological and Environmental Research and by the National Institutes of Health, National Institute of General Medical Sciences (including P41GM103393). The contents of this publication are solely the responsibility of the authors and do not necessarily represent the official views of NIGMS or NIH.

AUTHOR CONTRIBUTIONS

E.M.L. and J.M.K. wrote the manuscript. E.M.L., J.M.K., and D.R.H. solved the EM structures. J.A.E. and E.P.B. solved the crystal structure of ecCTPS. M.S. and J.M.H. generated disulfide cross-linked ecCTPS constructs and optimized purification and assembly conditions. E.M.L. and A.M. carried out CTPS activity assays. R.M.B. and Z.G. performed initial characterization of ecCTPS filaments. E.M.L., Z.G., E.P.B. and J.M.K. contributed to experimental design and data analysis and interpretation.

COMPETING FINANCIAL INTERESTS

The authors declare no competing financial interests.

1. Noree, C., Sato, B.K., Broyer, R.M. & Wilhelm, J.E. Identification of novel filament-forming proteins in *Saccharomyces cerevisiae* and *Drosophila melanogaster*. *J. Cell Biol.* **190**, 541–551 (2010).
2. Liu, J.L. Intracellular compartmentation of CTP synthase in *Drosophila*. *J. Genet. Genomics* **37**, 281–296 (2010).
3. Ingerson-Mahar, M., Briegel, A., Werner, J.N., Jensen, G.J. & Gitai, Z. The metabolic enzyme CTP synthase forms cytoskeletal filaments. *Nat. Cell Biol.* **12**, 739–746 (2010).
4. Carcamo, W.C. *et al.* Induction of cytoplasmic rods and rings structures by inhibition of the CTP and GTP synthetic pathway in mammalian cells. *PLoS One* **6**, e29690 (2011).
5. Shen, Q.J. *et al.* Filamentation of metabolic enzymes in *Saccharomyces cerevisiae*. *J. Genet. Genomics* **43**, 393–404 (2016).
6. Narayanaswamy, R. *et al.* Widespread reorganization of metabolic enzymes into reversible assemblies upon nutrient starvation. *Proc. Natl. Acad. Sci. USA* **106**, 10147–10152 (2009).
7. An, S., Kumar, R., Sheets, E.D. & Benkovic, S.J. Reversible compartmentalization of de novo purine biosynthetic complexes in living cells. *Science* **320**, 103–106 (2008).
8. Barry, R.M. *et al.* Large-scale filament formation inhibits the activity of CTP synthetase. *eLife* **3**, e03638 (2014).
9. Strochlic, T.I. *et al.* Ack kinase regulates CTP synthase filaments during *Drosophila* oogenesis. *EMBO Rep.* **15**, 1184–1191 (2014).

10. Petrovska, I. *et al.* Filament formation by metabolic enzymes is a specific adaptation to an advanced state of cellular starvation. *eLife* **3**, e02409 (2014).
11. Noree, C., Monfort, E., Shiau, A.K. & Wilhelm, J.E. Common regulatory control of CTP synthase enzyme activity and filament formation. *Mol. Biol. Cell* **25**, 2282–2290 (2014).
12. Chang, C.C. *et al.* Cytoophidium assembly reflects upregulation of IMPDH activity. *J. Cell Sci.* **128**, 3550–3555 (2015).
13. Chen, K. *et al.* Glutamine analogs promote cytoophidium assembly in human and *Drosophila* cells. *J. Genet. Genomics* **38**, 391–402 (2011).
14. Endrizzi, J.A., Kim, H., Anderson, P.M. & Baldwin, E.P. Crystal structure of *Escherichia coli* cytidine triphosphate synthetase, a nucleotide-regulated glutamine amidotransferase/ATP-dependent amidoligase fusion protein and homologue of anticancer and antiparasitic drug targets. *Biochemistry* **43**, 6447–6463 (2004).
15. Goto, M., Omi, R., Nakagawa, N., Miyahara, I. & Hirotsu, K. Crystal structures of CTP synthetase reveal ATP, UTP, and glutamine binding sites. *Structure* **12**, 1413–1423 (2004).
16. Endrizzi, J.A., Kim, H., Anderson, P.M. & Baldwin, E.P. Mechanisms of product feedback regulation and drug resistance in cytidine triphosphate synthetases from the structure of a CTP-inhibited complex. *Biochemistry* **44**, 13491–13499 (2005).
17. Kursula, P. *et al.* Structure of the synthetase domain of human CTP synthetase, a target for anticancer therapy. *Acta Crystallogr. Sect. F Struct. Biol. Cryst. Commun.* **62**, 613–617 (2006).
18. Lauritsen, I., Willemoës, M., Jensen, K.F., Johansson, E. & Harris, P. Structure of the dimeric form of CTP synthase from *Sulfolobus solfataricus*. *Acta Crystallogr. Sect. F Struct. Biol. Cryst. Commun.* **67**, 201–208 (2011).
19. Aughey, G.N. & Liu, J.L. Metabolic regulation via enzyme filamentation. *Crit. Rev. Biochem. Mol. Biol.* **51**, 282–293 (2016).
20. Aughey, G.N. *et al.* Nucleotide synthesis is regulated by cytoophidium formation during neurodevelopment and adaptive metabolism. *Biol. Open* **3**, 1045–1056 (2014).
21. Calise, S.J. *et al.* Glutamine deprivation initiates reversible assembly of mammalian rods and rings. *Cell. Mol. Life Sci.* **71**, 2963–2973 (2014).
22. Martin, E. *et al.* CTP synthase 1 deficiency in humans reveals its central role in lymphocyte proliferation. *Nature* **510**, 288–292 (2014).
23. Hofer, A., Steverding, D., Chabes, A., Brun, R. & Thelander, L. *Trypanosoma brucei* CTP synthetase: a target for the treatment of African sleeping sickness. *Proc. Natl. Acad. Sci. USA* **98**, 6412–6416 (2001).
24. Hindenburg, A.A., Taub, R.N., Grant, S., Chang, G. & Baker, M.A. Effects of pyrimidine antagonists on sialic acid regeneration in HL-60 cells. *Cancer Res.* **45**, 3048–3052 (1985).
25. Kang, G.J. *et al.* Cyclopentenylcytosine triphosphate. Formation and inhibition of CTP synthetase. *J. Biol. Chem.* **264**, 713–718 (1989).
26. Politi, P.M. *et al.* Phase I clinical trial of continuous infusion cyclopentenyl cytosine. *Cancer Chemother. Pharmacol.* **36**, 513–523 (1995).
27. Trudel, M., Van Genechten, T. & Meuth, M. Biochemical characterization of the hamster thy mutator gene and its revertants. *J. Biol. Chem.* **259**, 2355–2359 (1984).
28. Raushel, F.M., Thoden, J.B. & Holden, H.M. Enzymes with molecular tunnels. *Acc. Chem. Res.* **36**, 539–548 (2003).
29. Chang, Y.F., Martin, S.S., Baldwin, E.P. & Carman, G.M. Phosphorylation of human CTP synthetase 1 by protein kinase C: identification of Ser(462) and Thr(455) as major sites of phosphorylation. *J. Biol. Chem.* **282**, 17613–17622 (2007).
30. Choi, M.G. & Carman, G.M. Phosphorylation of human CTP synthetase 1 by protein kinase A: identification of Thr455 as a major site of phosphorylation. *J. Biol. Chem.* **282**, 5367–5377 (2007).
31. Choi, M.G., Park, T.S. & Carman, G.M. Phosphorylation of *Saccharomyces cerevisiae* CTP synthetase at Ser424 by protein kinases A and C regulates phosphatidylcholine synthesis by the CDP-choline pathway. *J. Biol. Chem.* **278**, 23610–23616 (2003).
32. Han, G.S. *et al.* Expression of Human CTP synthetase in *Saccharomyces cerevisiae* reveals phosphorylation by protein kinase A. *J. Biol. Chem.* **280**, 38328–38336 (2005).

ONLINE METHODS

Purification of ecCTPS. Wild-type ecCTPS was purified as described previously[3,14]. The ecCTPS^{CC} mutant was purified in the same manner, except 10-mM DTT was included throughout the purification.

Purification of hCTPS1. hCTPS1 was expressed in *Saccharomyces cerevisiae* strain GHY55, as described by Han *et al.*, 2005 (ref. 32). This strain lacks the endogenous *S. cerevisiae* CTPS genes URA7 and URA8, and contains plasmid pDO105-hCTPS1, which directs expression of His_6-tagged (C-terminal) hCTPS1 from the ADH1 promoter. GHY55 cells were grown in 4× YPD media and harvested by freezing cell pellets in liquid nitrogen. Cell pellets were ground to a powder while frozen, and 15 g of cell powder was resuspended in 100 mL of lysis buffer (50 mM Tris-HCl, 200 mM NaCl, 0.3M sucrose, 20 mM imidazole, 0.5 mM PMSF, pH 8.0). Lysates were clarified by centrifugation at 14,000 rpm for 40 min at 4 °C in a Thermo Scientific Fiberlite F14-14 × 50 cy rotor. Clarified lysates were applied to a 5 mL HisTrap FF Crude column (GE) on an ÄKTA Start chromatography system (GE), and the column was washed with 30 column volumes (CV) wash buffer (20 mM Tris-HCl, 0.5M NaCl, 45 mM imidazole, 10% glycerol, pH 7.9). Protein was eluted as 1-mL fractions with 5 CV elution buffer (20 mM Tris-HCl, 0.5M NaCl, 250 mM imidazole, 10% glycerol, pH 7.9). Fractions containing hCTPS1 were pooled and dialyzed into storage buffer (20 mM Tris-HCl, 0.5M NaCl, 10% glycerol, 7 mM β-mercaptoethanol, pH 7.9) using Snakeskin 3500 MWCO dialysis tubing (Thermo Scientific). Dialyzed protein was concentrated ~6-fold by centrifugation in a 3 kDa cut-off centrifugal filter unit (Millipore). hCTPS1 prepared for cryo-EM was purified in the same manner except protein was concentrated before dialysis and then dialyzed into 20 mM Tris-HCl, 50 mM NaCl, 7 mM β-mercaptoethanol, pH 7.9. The hCTPS1-H355A mutant was generated by site-directed mutagenesis of plasmid pDO105-hCTPS1 and purified in the same manner as WT hCTPS1.

Site-directed mutagenesis. Site-directed mutagenesis of the *E. coli* and human CTPS expression constructs was performed using the QuickChange (Agilent Technologies) and Q5 (NEB) systems, respectively.

CTPS activity assays. CTPS activity was determined at 37 °C by measuring ΔAbs_{291nm} over time using a NanoDrop 2000c spectrophotometer (Thermo Scientific). Absolute CTP production was calculated using the change in extinction coefficient between UTP and CTP at 291 nm (1338 $M^{-1}cm^{-1}$)[33]. k_{cat} values were determined from the initial linear region of the Abs_{291nm} versus time measurements. For ecCTPS, assays were performed with 0.5–2.5 μM ecCTPS or ecCTPS^{CC} in a standard reaction buffer containing 50 mM Na-HEPES (pH 8.0) and 10 mM $MgCl_2$, with or without 10 mM DTT as appropriate. Final substrate concentrations were 0.6 mM UTP, 1.5 mM ATP, 0.2 mM GTP and 10 mM glutamine or ammonia. Assays were carried out using the "annealing" method described by Habrian, *et al.*[34]: ecCTPS was incubated at 21 °C for 3 min and then combined with pre-warmed (37 °C) nucleotides. The enzyme-nucleotide mix was then incubated further for 4 min at 37 °C, after which pre-warmed glutamine or ammonia was added. The complete reaction mixture was then immediately transferred to a pre-warmed UV cuvette and ΔAbs_{291nm} over time measured at 37 °C. For hCTPS1, assays were performed with 8 μM hCTPS1 in a standard reaction buffer containing 20 mM Tris-HCl (pH 7.9) and 10 mM $MgCl_2$, with final substrate concentrations of 2 mM UTP, 2 mM ATP, 0.2 mM GTP, and 10 mM glutamine. The annealing method described above was also used for hCTPS1 activity assays, except the enzyme-nucleotide mix was incubated for 1 h at 37 °C to allow for hCTPS1 polymerization.

Negative-stain electron microscopy. Samples for negative-stain EM were prepared by applying CTPS to carbon-coated grids and staining with 0.7% uranyl formate. For ecCTPS^{CC}, protein was dialyzed overnight into 50 mM Na-HEPES (pH 8.0) with or without 10 mM DTT before being coated onto grids at a final concentration of 2.5 μM. For hCTPS1 and hCTPS1-H355A, samples were prepared with 2.5 μM protein in 20 mM Tris-HCl (pH 7.9) and 10 mM $MgCl_2$, supplemented with appropriate nucleotides at the following concentrations: UTP (2 mM), ATP (2 mM), AMP-PNP (2 mM), GTP (0.2 mM), ADP (2 mM), and CTP (2 mM). hCTPS1 was incubated with nucleotides for 1 h at 37 °C before being coated onto grids. For depolymerization experiments, glutamine (10 mM) was added following incubation with nucleotides, and negative-stain samples were prepared 30 and 120 min following glutamine addition. EM was performed on a Tecnai G2 Spirit (FEI co.) operating at 120 kV, and images were acquired at 52,000× magnification on a US4000 4k × 4k CCD camera (Gatan, Inc.).

Cryo-electron microscopy. Samples for cryo-EM were prepared by applying protein to glow-discharged C-Flat holey-carbon grids (Protochips Inc.), blotting with a Vitrobot (FEI co.), and rapidly plunging into liquid ethane. For ecCTPS^{CC}, protein was dialyzed into nonreducing buffer (50 mM Na-HEPES pH 8.0) to promote filament assembly. Samples for cryo-EM were then prepared with 2.5 μM ecCTPS^{CC} in the absence of nucleotides or following 1 h incubation of filaments with 10 mM $MgCl_2$ in addition to UTP (0.6 mM) and ATP (1.5 mM) or CTP (0.6 mM) and ADP (1.5 mM). hCTPS1 (5 μM) was incubated for 1 h with 10 mM $MgCl_2$, 2 mM UTP, 2 mM ATP, and 0.2 mM GTP before preparing cryo-EM samples. For ecCTPS tetramers, 5 μM ecCTPS was incubated with 10 mM $MgCl_2$, 0.6 mM UTP, 1.5 mM AMP-PNP, 0.2 mM GTP and 10 mM glutamine before preparing cryo-EM samples. Cryo-EM data for the wild-type ecCTPS filament were acquired in a Tecnai Polara operating at 300 kV and recorded on a K2 Summit Direct Detect camera with a total dose of ~34 $e^-/Å^2$ with 36 frames per exposure. For all other samples, cryo-EM data was collected on a Tecnai G2 F20 (FEI co.) operating at 200 kV with a K2 Summit Direct Detect camera (Gatan Inc.) with a pixel size of 1.26 Å/pixel. Movies were acquired in counting mode with 36 frames and a total dose of ~45 $e^-/Å^2$ (filaments) or ~68 $e^-/Å^2$ (ecCTPS tetramers), and with a defocus range between 0.8 and 2.5 μm (filaments) or 1.0 and 4.5 μm (ecCTPS tetramers). Leginon software[35] was used to automate data collection.

Image processing and 3D reconstruction. Movie frames were aligned using DOSEFGPU DRIFTCORR[36] and CTF parameters were estimated using CTFFIND3 (ref. 37). For helical samples, lengths of helices were manually defined using Appion[38] manual picker, and overlapping segments were extracted along the length of each helix. Particle stacks were CTF corrected by phase flipping in SPIDER[39], using parameters determined by CTFFIND3. 3D reconstruction of helices was performed by iterative helical real space reconstruction (IHRSR)[40,41] in SPIDER, using hsearch_lorentz[42] to refine helical symmetry parameters. Cylinders were used as starting models, and the D2 point-group symmetry of the CTPS tetramer was enforced. Iterative gold-standard refinement was performed with increasingly smaller angular increments (minimum 1.5°). For single-particle (tetramer) samples, particles were picked automatically using DoG Picker[43] and then extracted using Appion. Relion[44] was used for CTF correction (using CTFFIND3 parameters) and subsequent classification and refinement. We performed reference-free 2D classification and selected 7,700 and 39,000 particles for 3D classification of the hCTPS1-H355A and ecCTPS tetramers, respectively. For 3D classification, initial reference volumes were generated from the homology model of the hCTPS1 tetramer or crystal structure of the product-bound ecCTPS tetramer. Both reference volumes were low-pass filtered to 60 Å, and D2 symmetry was enforced during 3D classification. Following 3D classification, 4,400 and 6,400 particles were selected for hCTPS1-H355A and ecCTPS, respectively, for gold-standard 3D refinement. Again, reference volumes were low-pass filtered to 60 Å and D2 symmetry was enforced during 3D refinement. The gold-standard FSC = 0.143 criterion was used for estimating resolution. Raw volumes were amplitude corrected and low and high-pass filtered using SPIDER. Details of each 3D reconstruction are summarized in **Table 1**.

Building and fitting of atomic models. An ecCTPS monomer (PDB 2AD5) was initially fit as a single rigid body into the cryo-EM structure of the filament. For the human filament, an initial homology model of the full-length hCTPS monomer was generated from the crystal structures of the individual domains (PDB 2VO1 and 2VKT) aligned to ecCTPS (PDB 2AD5) using MODELLER[45] then fit to cryo-EM density as three rigid bodies: GAT domain, linker domain, and ALase domain. For both structures, atomic models were refined with the Rosetta Relax application[46], using the cryo-EM density as a constraint. Adjacent protomers within the tetramer and at filament contact sites were included during the Relax procedure to allow for refinement at subunit interfaces.

X-ray structure of an alternate CTP-inhibited ecCTPS conformation. N-terminal His-tagged ecCTPS mutant C268A was expressed and purified using metal chelate chromatography as previously described[16]. ecCTPS(C268A) had identical k_{cat}

and CTP inhibition as wild type. Protein for crystallization was stored in 10 mM Tris-Cl, 0.5 mM TCEP, pH 8.0 at −80 °C at 10–15 mg/mL. $P2_12_12$ crystals isomorphous to the published apo- and CTP/ADP-liganded structures (PDB 1S1M and 2AD5) were grown using vapor diffusion from 7.5 mg/mol ecCTPS-C268A, 0.8–1.2 M ammonium sulfate, 0.1 M Tris-Cl, pH 8.0 as previously described[14] with drops supplemented with 5 mM CTP, 5 mM magnesium sulfate and 10 mM glutamine. For cryoprotection, crystals were briefly rinsed in 1:1 mixture of 50% MPD: mother liquor (25% MPD final), wicked and flash cooled in liquid nitrogen. Reflection data were acquired at Stanford Synchrotron Radiation Lightsource Beamline 1-5 at 100 K at a wavelength of 0.979610 Å and 1° oscillation/image, using a ADSC Quantum 315 detector. 88 frames were processed using DENZO/Scalepack (HKL2000 package). Phases were derived from the water-free published CTP and ADP complex structure (PDB 2AD5). Maximum-likelihood structure factor refinement was carried out on nonhydrogen atoms using Refmac 5.6 with Babinet scaling with an anisotropic *B*-factor correction (BSOL fixed at 125.00 and final anisotropic scaling parameters B11 = −1.82, B22 = 2.83, B33 = −1.01, B12 = 0.00, B13 = 0.00, B23 = 0.00). Quaternary changes were accounted for by initial rigid-body refinement for individual monomers and then for three separate domains of each monomer (1–266, 267–287, 288–544). Cycles of manual model building with Coot 0.6.2 and combined positional and *B*-factor refinement led to the final model. The distribution of favored, allowed, and outlier Ramachandran angles were 94, 5 and 1%, respectively (51st percentile for structures at this resolution). The data collection and final model statistics are provided in **Table 2**.

Sequence comparison. CTPS sequences were obtained from BLAST searches[47], and multiple sequence alignments of several hundred sequences were performed with MAFFT[48].

Data availability. Coordinates and structure factors for the CTP-inhibited ecCTPS crystal structure have been deposited in the Protein Data Bank under accession code PDB 5TKV. EM structures and associated atomic models have been deposited in the Electron Microscopy Data Bank and Protein Data Bank with the following accession codes: ecCTPS filament (EMD-8504; PDB 5U3C), hCTPS1 filament (EMD-8474; PDB 5U03), hCTPS1-H355A tetramer (EMD-8476), ecCTPS tetramer (EMD-8475; PDB 5U05), ecCTPS-CC (apo) (EMD-8490), ecCTPS-CC (substrates) (EMD-8491), ecCTPS-CC (products) (EMD-8513; PDB 5U6R). Other data supporting this study are available from the corresponding authors upon reasonable request.

33. Long, C.W. & Pardee, A.B. Cytidine triphosphate synthetase of *Escherichia coli* B. I. Purification and kinetics. *J. Biol. Chem.* **242**, 4715–4721 (1967).
34. Habrian, C. *et al.* Inhibition of *Escherichia coli* CTP synthetase by NADH and other nicotinamides and their mutual interactions with CTP and GTP. *Biochemistry* **55**, 5554–5565 (2016).
35. Suloway, C. *et al.* Automated molecular microscopy: the new Leginon system. *J. Struct. Biol.* **151**, 41–60 (2005).
36. Li, X. *et al.* Electron counting and beam-induced motion correction enable near-atomic-resolution single-particle cryo-EM. *Nat. Methods* **10**, 584–590 (2013).
37. Mindell, J.A. & Grigorieff, N. Accurate determination of local defocus and specimen tilt in electron microscopy. *J. Struct. Biol.* **142**, 334–347 (2003).
38. Lander, G.C. *et al.* Appion: an integrated, database-driven pipeline to facilitate EM image processing. *J. Struct. Biol.* **166**, 95–102 (2009).
39. Frank, J. *et al.* SPIDER and WEB: processing and visualization of images in 3D electron microscopy and related fields. *J. Struct. Biol.* **116**, 190–199 (1996).
40. Egelman, E.H. The iterative helical real space reconstruction method: surmounting the problems posed by real polymers. *J. Struct. Biol.* **157**, 83–94 (2007).
41. Sachse, C. *et al.* High-resolution electron microscopy of helical specimens: a fresh look at tobacco mosaic virus. *J. Mol. Biol.* **371**, 812–835 (2007).
42. Egelman, E.H. A robust algorithm for the reconstruction of helical filaments using single-particle methods. *Ultramicroscopy* **85**, 225–234 (2000).
43. Voss, N.R., Yoshioka, C.K., Radermacher, M., Potter, C.S. & Carragher, B. DoG Picker and TiltPicker: software tools to facilitate particle selection in single particle electron microscopy. *J. Struct. Biol.* **166**, 205–213 (2009).
44. Scheres, S.H. RELION: implementation of a Bayesian approach to cryo-EM structure determination. *J. Struct. Biol.* **180**, 519–530 (2012).
45. Webb, B. & Sali, A. Comparative protein structure modeling using MODELLER. *Curr. Protoc. Bioinformatics* **54**, 5.6.1–5.6.37 (2016).
46. DiMaio, F. *et al.* Atomic-accuracy models from 4.5-Å cryo-electron microscopy data with density-guided iterative local refinement. *Nat. Methods* **12**, 361–365 (2015).
47. Johnson, M. *et al.* NCBI BLAST: a better web interface. *Nucleic Acids Res.* **36**, W5–W9 (2008).
48. Katoh, K. & Standley, D.M. MAFFT multiple sequence alignment software version 7: improvements in performance and usability. *Mol. Biol. Evol.* **30**, 772–780 (2013).

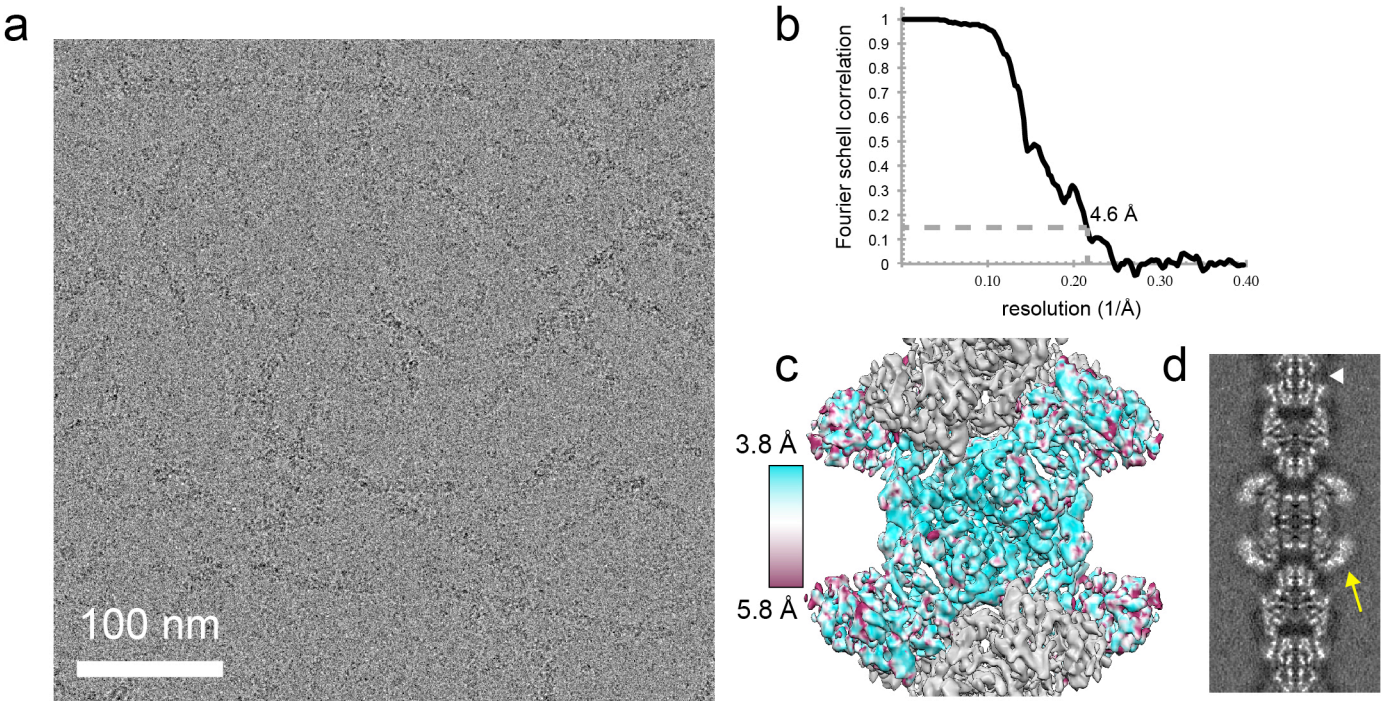

Supplementary Figure 1

Cryo-EM reconstruction of ecCTPS.

a, Cryo-electron micrograph of ecCTPS filaments. **b,** The resolution of the structure is 4.6 Å by gold-standard FSC. **c,** Local resolution map of one ecCTPS tetramer in the filament. **d,** A central slice through the unfiltered ecCTPS filament reconstruction shows less well-defined features in the GAT domains (yellow arrow) than in the AL domains (white arrowhead).

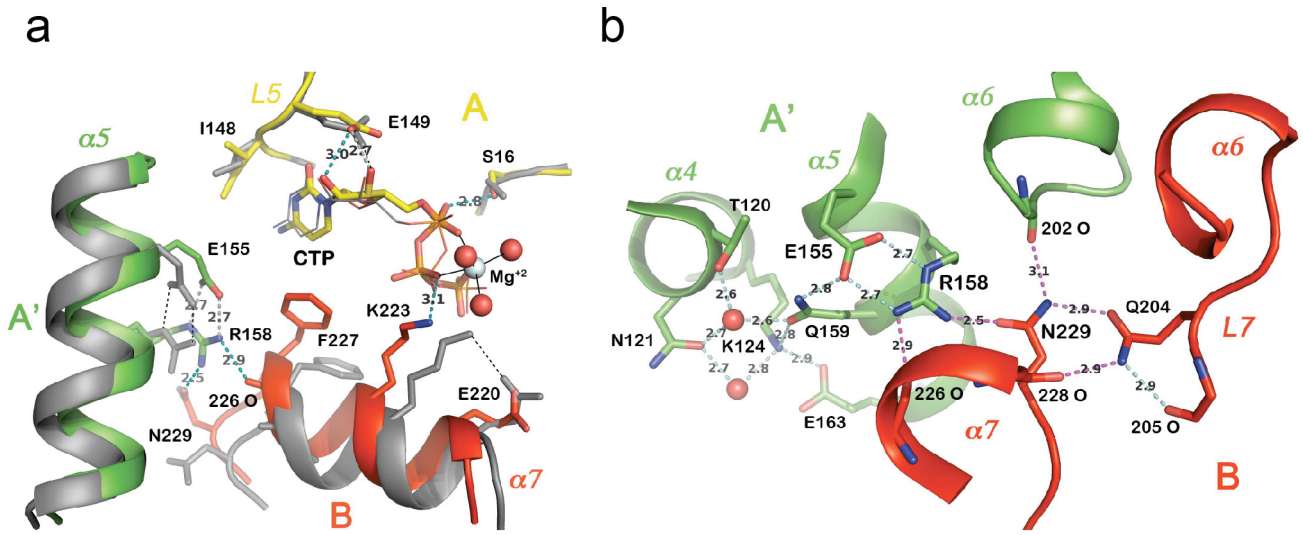

Supplementary Figure 2

Details of structural rearrangements at the CTP binding site that create new intersubunit contacts and drive the conformational switch to the filament-forming conformer.

a, The alternative ecCTPS-CTP complex structure (5TKV) is shown in yellow (subunit A), red (subunit B) and green (subunit A', two-fold symmetry related to A, symmop 4). The previously published CTP complex (2AD5[16]) is shown in gray, after superposition of the A subunits (residues 1-266, 0.42 Å Cα rmsd after superposition). Side chains that have altered interactions or conformations relative to 2AD5 are displayed. Hydrogen bonds unique to 5TKV are shown as cyan dotted lines, and heavy atom distances are indicated. The 2AD5 CTP is depicted using narrow sticks. In 5TKV, an octahedral Mg^{+2} ion coordinates the β- and γ-phosphate oxygens and 3 water molecules. Relative to the A subunit, helices α5(A') and α7(A) Cα atoms shifted 1.9 Å and 1.1 Å respectively. F227 and N229 side chains changed rotamers, with the F227 phenyl ring packed against the CTP C5 atom, while N229 formed new inter-subunit hydrogen bonds with R158. These new hydrogen bonds became possible due to a quaternary rearrangement of subunits that was similar to the rearrangement of N-terminal domains in the filament-binding conformer observed by cryoEM. This structure validates the sequence conservation for these residues. Mutations at E155, R158 and position 229 confer pyrimidine drug resistance in CTPSs, presumably by hindering the conformational change required for formation of the filament (bacterial[49]) or inhibited tetramer (yeast[50], mammalian[51]). Similar intersubunit contacts are observed in tetramer crystal structures of the *M. tuberculosis* CTPS-diUTP complex (PDB 4ZDJ), *T. thermophilus* CTPS-glutamine (PDB 1VCO) and apo (PDB 1VCM) complexes, and the hCTPS1 AL domain (PDB 2VO1). **b,** E155 and N229 participate in extended hydrogen bond networks in the A' and B subunits. Hydrogen bonds specific to 5TKV are depicted in magenta, while those common to both 2AD5 and 5TKV are colored light blue. R158 and N229 form the center of this network.

49. Wylie, J.L., Wang, L.L., Tipples, G. & McClarty, G. A single point mutation in CTP synthetase of Chlamydia trachomatis confers resistance to cyclopentenyl cytosine. *J Biol Chem* **271**, 15393-400 (1996).
50. Ostrander, D.B., O'Brien, D.J., Gorman, J.A. & Carman, G.M. Effect of CTP synthetase regulation by CTP on phospholipid synthesis in Saccharomyces cerevisiae. *J Biol Chem* **273**, 18992-9001 (1998).
51. Whelan, J., Phear, G., Yamauchi, M. & Meuth, M. Clustered base substitutions in CTP synthetase conferring drug resistance in Chinese hamster ovary cells. *Nat Genet* **3**, 317-22 (1993).

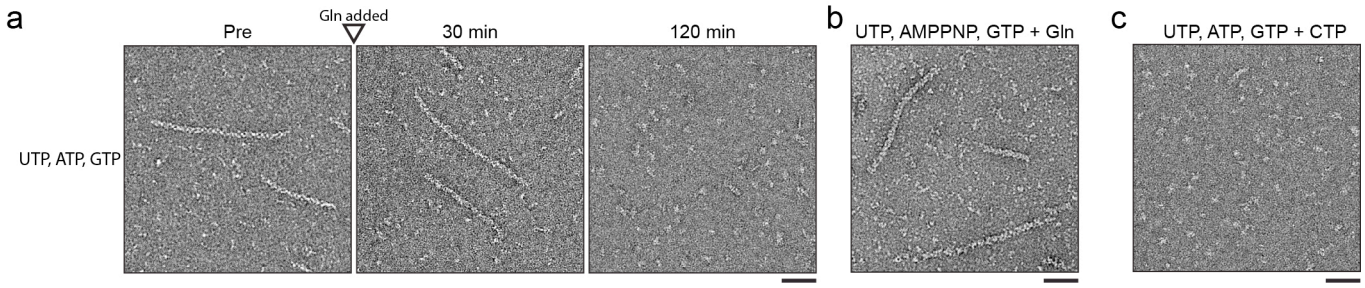

Supplementary Figure 3

CTP promotes disassembly of hCTPS1 filaments.

a, Adding glutamine to hCTPS1 filaments assembled with UTP, ATP, and GTP causes them to disassemble over time. **b**, Adding glutamine to hCTPS1 filaments assembled with UTP, AMPPNP, and GTP does not lead to filament disassembly, suggesting CTP synthesis is required to promoted hCTPS1 depolymerization. **c**, Directly adding CTP to hCTPS1 filaments assembled with UTP, ATP, and GTP causes filaments to disassemble. Scale bars are 50 nm.

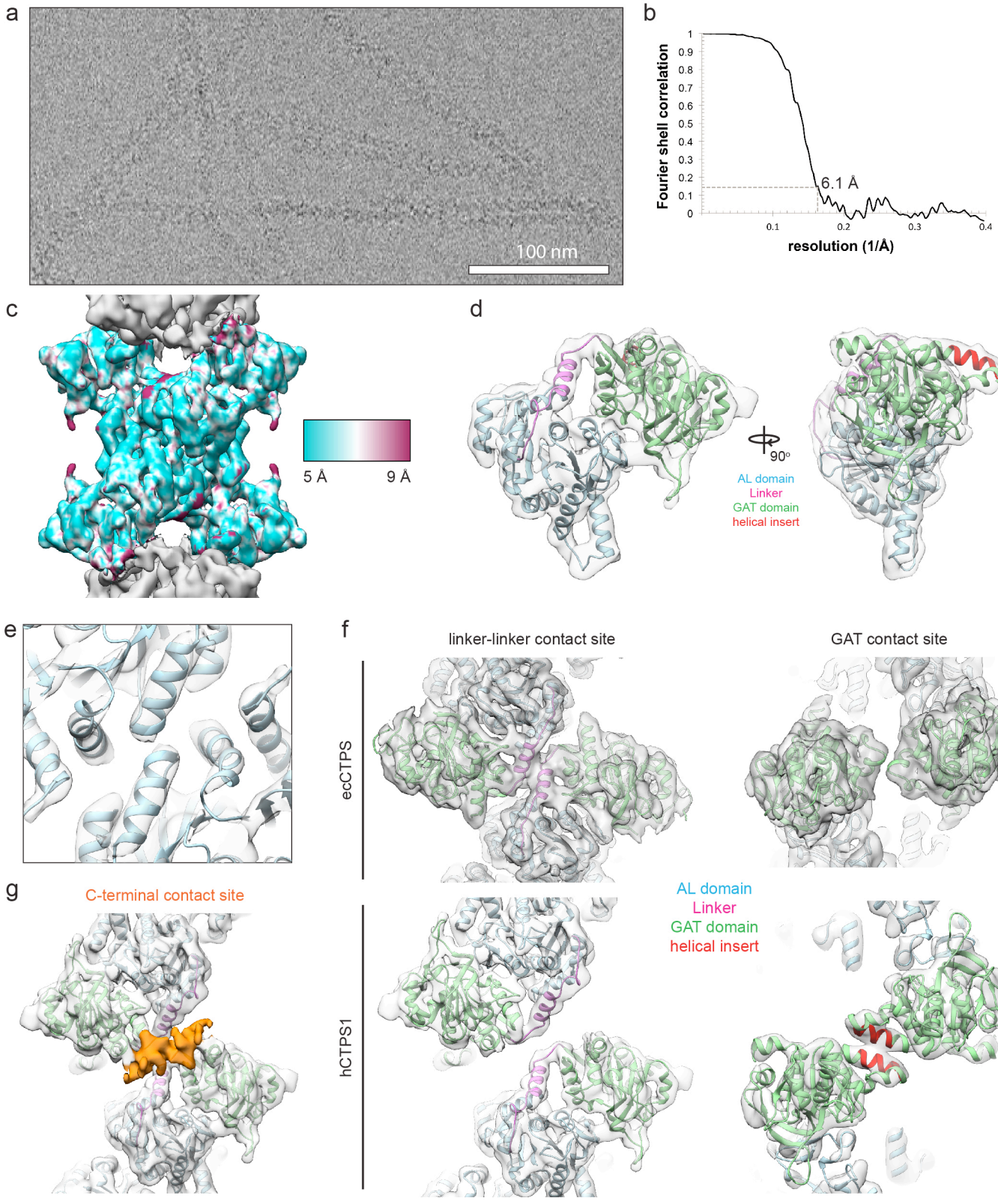

Supplementary Figure 4

Cryo-EM reconstruction of hCTPS1.

a, Section from a micrograph of frozen hCTPS1. **b,** FSC curve for the hCTPS1 filament, showing a resolution of 6.1Å. **c,** ResMap local resolution map of the hCTPS1 filament. **d,** Atomic model of the hCTPS1 monomer fit into the hCTPS1 filament cryoEM map, colored by domain. **e,** Individual helices are well-defined in the hCTPS1 filament cryoEM map. **f,** Comparison of the ecCTPS and hCTPS1 filament contact sites. hCTPS1 filaments lack the linker-linker contact site, and have a completely rearranged GAT contact site. **g**, Poorly-resolved C-terminal contact site (orange) in the hCTPS1 filament.

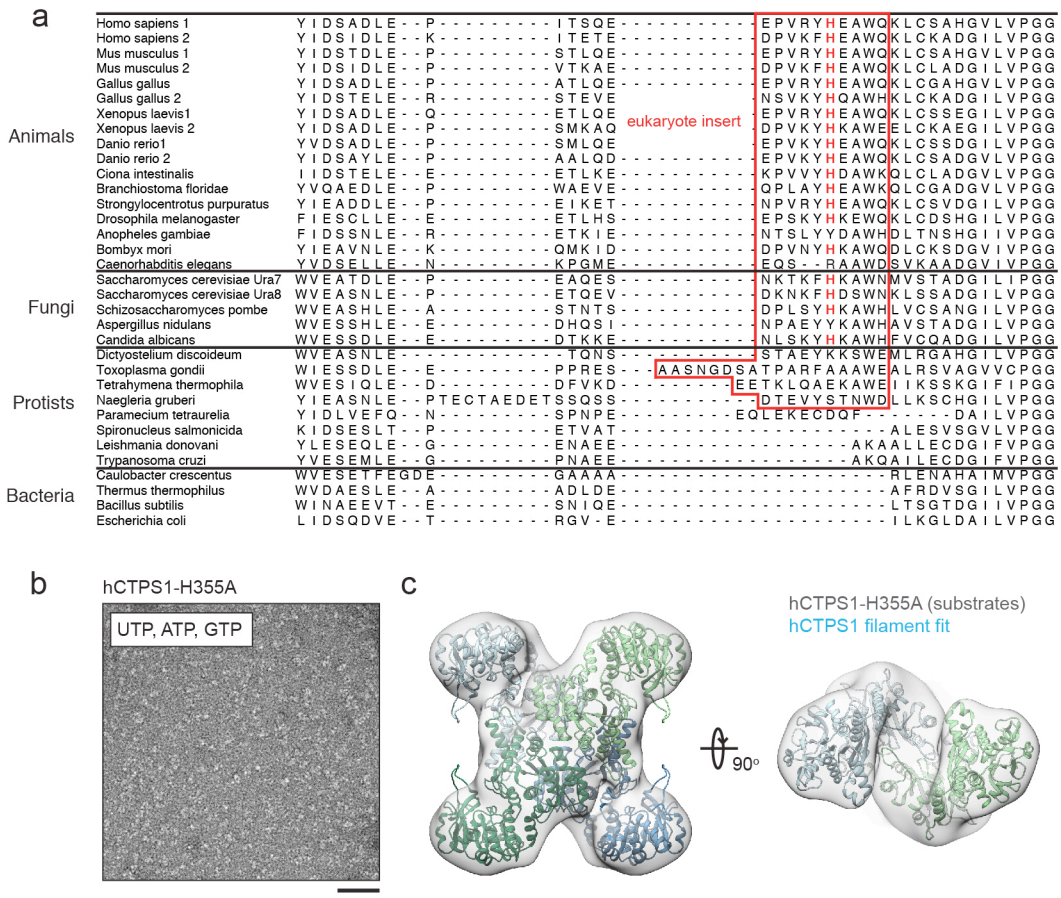

Supplementary Figure 5

Mutation of a conserved histidine in the eukaryotic GAT-domain insert abolishes hCTPS1 polymerization without disrupting tetramer formation.

a, CTPS sequence alignments, showing the appearance of the GAT domain helical insert early in eukaryotic evolution. The conserved histidine (H355 in humans) is shown in red. **b**, hCTPS1-H355A does not polymerize in the presence of UTP, ATP, and GTP. **c**, Negative stain reconstruction of the hCTPS1-H355A tetramer in the presence of substrates (grey), fit with an atomic model of hCTPS1 in the filament conformation (colored by protomer). Scale bar is 50 nm.